# Effects of coverage on the geometry and electronic structure of Al overlayers on Si(111)

R. J. Hamers
*IBM Research Division, Thomas J. Watson Research Center, P.O. Box 218, Yorktown Heights, New York 10598*
(Received 25 January 1989)

Scanning tunneling microscopy (STM) has been used to study the coverage dependence of the atomic geometry and electronic structure of ordered overlayers of aluminum on Si(111). STM results for the Si(111)-($\sqrt{3}\times\sqrt{3}$)Al, Si(111)-($\sqrt{7}\times\sqrt{7}$)Al, and Si(111)-(7×7)Al overlayers, at $\frac{1}{3}$, $\frac{3}{7}$, and 1 monolayer (ML) Al coverage, identify changes in the local Al bonding sites associated with the different surface symmetry and local Al coverage. A hitherto unreported (2×1) structure is also observed coexisting with both $\sqrt{3}\times\sqrt{3}$ and $\sqrt{7}\times\sqrt{7}$ structures. The results confirm a threefold adatom geometry for the $\sqrt{3}\times\sqrt{3}$ surface, and reveal clusters of threefold Al adatoms adsorbed on twofold sites for the $\sqrt{7}\times\sqrt{7}$ surface and the substitution of Al for Si in the outer double layer for the (7×7)Al surface. The transition from semiconducting to metallic behavior is directly correlated with changes in the local bonding geometry as a function of coverage.

## I. INTRODUCTION

The atomic structure and bonding of metal overlayers on semiconductor surfaces have been widely studied to better understand metal-semiconductor interfaces. The Al/Si(111) system is particularly interesting since several different ordered phases can be formed with increasing Al coverage under otherwise identical preparation conditions,[1–4] thereby allowing one to study the effect of surface coverage on the bonding sites adopted by the Al atoms. Additionally, the relatively simple electronic structure of aluminum has permitted detailed electronic-structure and total-energy calculations to be performed for a number of possible bonding geometries.[1–4] Experimental structure determinations on these various overlayers have been somewhat less successful. Lander and Morrison[5] used low-energy electron diffraction (LEED) to first identify the various phases and their surface symmetries as a function of coverage and substrate temperature. With the exception of the ($\sqrt{3}\times\sqrt{3}$) structure, which has been widely studied both theoretically and experimentally, the other phases exhibited complex behavior which has precluded an analysis of their structures. Experimental structural determinations have been further complicated by the coexistence of multiple phases, making it difficult to identify the properties of any single phase with most experimental techniques, particularly those based on electron diffraction.[5] However, the real-space nature of tunneling microscopy makes it possible to study the properties of each overlayer separately.

In this paper, the results of scanning-tunneling-microscopy (STM) experiments on Al-induced overlayers on Si(111) at coverages between 0 and 1 monolayer (ML) are presented. Starting with clean Si(111)-(7×7), Al-induced overlayers having ($\sqrt{3}\times\sqrt{3}$)$R$30°, ($\sqrt{7}\times\sqrt{7}$)$R$19.1°, (7×7), and (2×1) symmetry have been observed in STM. STM results on each of these overlayers will be presented first, beginning with the lowest-coverage structure. For the higher-coverage overlayers, particular emphasis is placed on images obtained at phase and domain boundaries, as such images can provide valuable information about the relative translational and rotational orientations of different phases, which is otherwise difficult to obtain. In the particular case of the $\sqrt{3}\times\sqrt{3}$ structure, emphasis is also placed on the geometry and electronic structure of naturally occurring point defects, as here an understanding of the nature of the surface *imperfections* also sheds light on the nature of the perfect surface.

## II. EXPERIMENT

The scanning tunneling microscope used in this study was described previously.[6] Tunneling results were obtained on all overlayers on both 6-mΩ cm $n$-type (Sb-doped) wafers and 5-mΩ cm $p$-type (B-doped) wafers, with equivalent results. Prior to deposition of aluminum, these wafers were carefully out-gassed and annealed by resistance heating. All samples initially showed large, well-ordered regions of Si(111)-(7×7). Aluminum was then deposited from an Al-coated tungsten filament using a quartz-crystal thickness monitor to measure the coverage; absolute coverages were determined by calibrating the quartz monitor using Rutherford backscattering. The surface symmetry was also measured using LEED.

Previous studies have identified numerous ordered overlayers of Al on Si(111) depending on Al coverage and substrate temperature. The procedures followed here closely follow those initially reported by Lander and Morrison.[5] The Si(111)-($\sqrt{3}\times\sqrt{3}$)$R$30°-Al surface was prepared either by depositing 2 ML of Al onto Si(111)-(7×7) followed by heating to 1175 K for 1 min or by depositing $\frac{1}{3}$ ML Al onto the hot (875 K) Si(111)-(7×7) surface. Deposition onto the hot surface generally produced overlayers with a higher degree of long-range order. The Si(111)-($\sqrt{7}\times\sqrt{7}$)$R$19.1°-Al overlayer was prepared by heating the ($\sqrt{3}\times\sqrt{3}$) surface to 875 K and depositing an additional $\simeq\frac{1}{5}$ ML Al. The $\sqrt{3}\times\sqrt{3}$ and $\sqrt{7}\times\sqrt{7}$

 

overlayers coexist with relative abundances determined by the exact amount of Al deposited. A $(2\times1)$ structure, which has not been previously reported, was also observed coexisting with $\sqrt{3}\times\sqrt{3}$ and $\sqrt{7}\times\sqrt{7}$ overlayers. Finally, the high-coverage Si(111)-$(7\times7)$Al surface was formed by depositing 1–2 ML Al and heating to 975 K.

After preparing these surfaces, the samples were cooled for approximately 60 min in ultrahigh vacuum in order to reduce thermal drift in the STM. Constant-current topographs were recorded under a variety of sample-biasing conditions in order to probe both the occupied and unoccupied electronic states. To provide density-of-states (DOS) information, constant-separation $I$-$V$ curves were measured simultaneously with the topographs via the current-imaging tunneling-spectroscopy (CITS) method.[7] The STM tips were cleaned by thermal annealing, which greatly improves the reproducibility of the tunneling-spectroscopy data. In some cases, the spectroscopy data were averaged over many unit cells to provide a comparison with other experimental and theoretical results. The spectroscopy data are presented as plots of $(V/I)(dI/dV)$ versus $V$. This provides a convenient normalization for the spectroscopy (equal to unity at $V=0$). Previous studies have demonstrated a good correspondence between peaks in $(V/I)(dI/dV)$ and peaks in the surface density of states.[8–10]

## III. RESULTS

### A. Si(111)-$(\sqrt{3}\times\sqrt{3})$Al

#### *1. STM images topographs of ideal surfaces*

Since its first observation in LEED,[5] this phase has been widely studied both experimentally and theoretically as a prototypical metal-on-semiconductor system.[1,11–15] Figure 1 shows STM topographic images of the $\sqrt{3}\times\sqrt{3}$ structures of Al/Si(111) acquired at a positive sample bias (+2 V), where electrons tunnel into empty electronic states of the surface. Also included in this image is a boundary between two domains. Images of the "ideal" $\sqrt{3}\times\sqrt{3}$ surface acquired at negative sample bias (not shown) appear identical to those obtained at positive bias (as in Fig. 1), except that the magnitude of the STM corrugations are always much larger at positive sample bias (1.2 Å at +2 V) than at negative bias (0.35 Å at −2 V). The magnitudes of the corrugations are not strongly dependent on the magnitude of these voltages, but primarily on the polarity. This pronounced difference in corrugation amplitude indicates that the unoccupied electronic states are much more strongly localized than the occupied states, thereby giving rise to larger corrugations.

Previous studies have suggested that more than one structure with $\sqrt{3}\times\sqrt{3}$ symmetry might be formed.[5,14] Measurements of the relative atomic positions on both sides of $(\sqrt{3}\times\sqrt{3})$-$(\sqrt{3}\times\sqrt{3})$ domain boundaries were used to evaluate whether multiple adsorption sites might be present for the $\sqrt{3}\times\sqrt{3}$ overlayer. Figure 1(b) shows the same sample images as Fig. 1(a), but now with a hexagonal lattice superimposed. It is clear from this image that the $\sqrt{3}\times\sqrt{3}$ domains on each side of the boundary show protrusions located on the same site relative to the underlying Si(111) lattice. Repeated measurements at other boundaries demonstrate that the preparation conditions used here lead to a unique $\sqrt{3}\times\sqrt{3}$ overlayer structure.

As a result of the overall sixfold symmetry and the lack

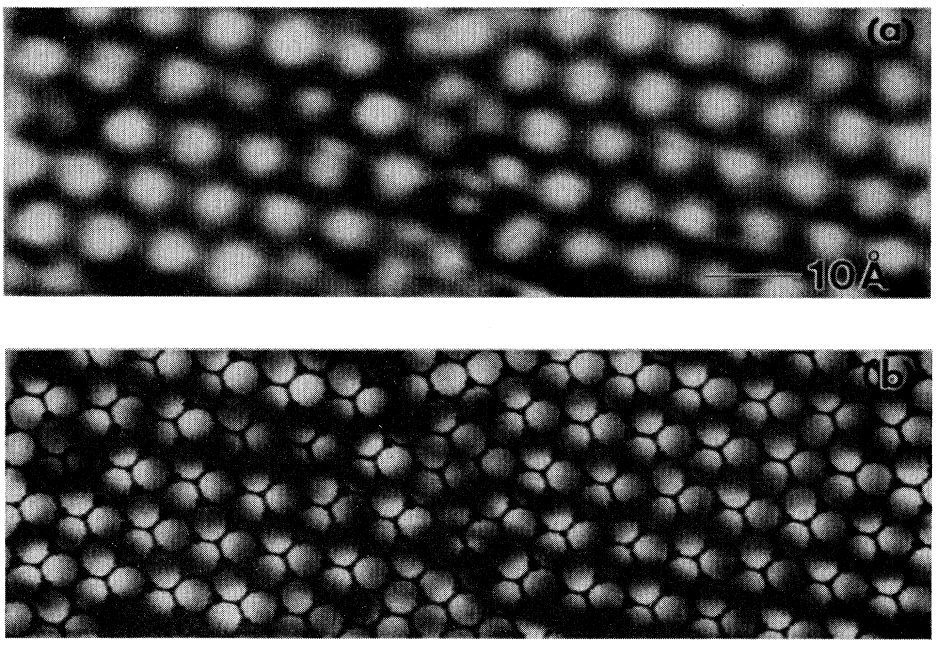


FIG. 1. (a) STM topographic images of Si(111)-$(\sqrt{3}\times\sqrt{3})$Al including a boundary between two domains. (b) Same image as in (a), but now with a hexagonal lattice superimposed.

of observable structure within the individual $\sqrt{3}\times\sqrt{3}$ unit cells, these separate images of the $\sqrt{3}\times\sqrt{3}$ structure leave unanswered the question of whether the protrusions observed at positive and negative bias arise from the same locations or exhibit a lateral shift, which might be produced by a spatial separation of empty and filled states. Images taken over larger distance scales routinely show individual point defects within the overlayer, which will be discussed in detail below. These point defects serve as reference points for comparing images of the $\sqrt{3}\times\sqrt{3}$ overlayer at both positive and negative bias. By comparing images taken over identical regions at positive and negative bias and later overlaying them such that the defects overlap, it can be conclusively shown that the protrusions characteristic of the ordered $(\sqrt{3}\times\sqrt{3})$Al overlayer at positive and negative bias are *coincident*. A similar conclusion is reached from local tunneling-spectroscopy measurements, as reported previously.[16] The measurements and the voltage-dependent STM imaging results demonstrate that the protrusions observed in constant-current STM are primarily geometric in origin. Yet, the greater magnitude of the corrugations at positive bias than at negative bias also indicates that electronic structure plays an important role in the STM imaging process.

### 2. *Defects in the $\sqrt{3}\times\sqrt{3}$ structure*

The dominant feature of the ideal $\sqrt{3}\times\sqrt{3}$ overlayer is the single protrusion observed in each unit cell. In addition, two types of characteristic defects are observed, as shown in Fig. 2.

The first type, labeled $V$ in Fig. 2, is attributed to a vacancy and appears as a depression $\simeq 1.5$ Å lower than the average height of the $\sqrt{3}\times\sqrt{3}$ overlayer, both at positive and negative sample bias. Essentially the same height change is observed when several vacancies cluster together. Since to first order the tip path follows a contour of constant electronic-state density (here, for unoccupied states), this indicates that the unoccupied states of the $\sqrt{3}\times\sqrt{3}$ overlayer project $\simeq 1.5$ Å higher than those of the underlying Si(111) double layer.

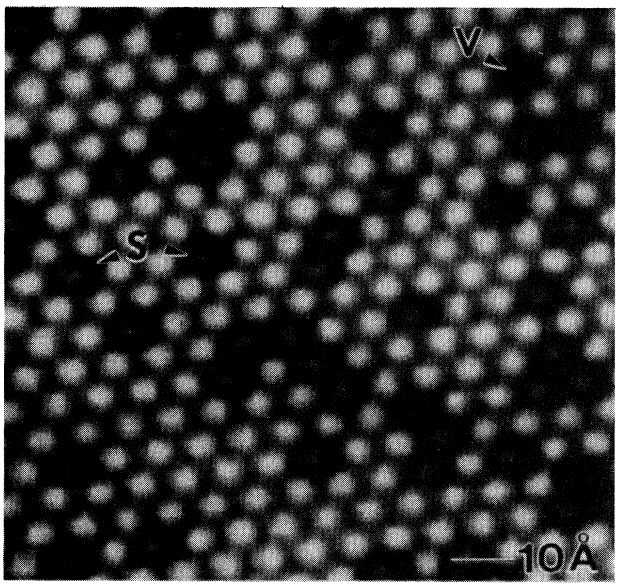


FIG. 2. STM topographic image of Si(111)-$(\sqrt{3}\times\sqrt{3})$Al including Si substitutional defects (+1.2 eV sample bias).

The second and more common defect is attributed to a substitutional defect, labeled $S$ in Fig. 2. The appearance of these defects is strongly dependent on the sign of the applied tunnel bias potential, indicating that their electronic structure is quite different from that of the ideal $\sqrt{3}\times\sqrt{3}$ overlayer. At both positive and negative sample bias, the substitutional defects appear as protrusions in the same place as a normal $(\sqrt{3}\times\sqrt{3})$Al unit cell would, but with a significantly different height. At positive sample bias (tunneling into the sample), as in Fig. 2, the protrusion at each defect is $\simeq 1$ Å *lower* than that of the $(\sqrt{3}\times\sqrt{3})$Al cell. At negative sample bias (tunneling out of the sample) the protrusion at each defect is $\simeq 1$ Å *higher* than those for $(\sqrt{3}\times\sqrt{3})$Al.

These substitutional defects are identified as silicon atoms on the basis of coverage-dependent measurements which show that their number is inversely correlated with the Al coverage between 0 and $\frac{1}{3}$ ML. Previous studies have indicated that the $\sqrt{3}\times\sqrt{3}$ structure may arise from aluminum adatoms in threefold sites atop a bulklike Si(111) lattice.[1,5,13] In this case, $\frac{1}{3}$ ML Al is required to saturate all Si dangling bonds. Since at $\frac{1}{6}$ ML Al only half of the dangling bonds of the Si(111) surface will be saturated, one might expect the remaining sites to be occupied by silicon adatoms in order to minimize the number of dangling bonds, in analogy with the structure adopted by the clean Si(111)-(7×7) surface.

This is indeed the case, as shown in Fig. 3. Here, STM topographs were acquired over a single region, but with the sample-bias polarity changed between the two images, of a sample with $\Theta_{\mathrm{Al}}=\frac{1}{6}$ ML. In both cases, protrusions of two discrete heights are observed. The images are also complementary in the sense that those atoms which appear as protrusions in the first image appear as depressions in the second, and vice versa. This structure can be well described as a $\sqrt{3}\times\sqrt{3}$ "surface alloy" of Al and Si adatoms, in which the atoms bond to the surface in an ordered $\sqrt{3}\times\sqrt{3}$ array, but with the chemical identity varying between Al and Si in an irregular manner. As the Al coverage is increased, the ratio of Al and Si adatoms is observed to change in a continuous manner until at $\simeq\frac{1}{3}$ ML Al, where the $\sqrt{3}\times\sqrt{3}$ structure is well formed, approximately 5–10 % of the surface atoms are actually Si-substitutional defects. At still slightly higher coverage, the $\sqrt{7}\times\sqrt{7}$ structure (discussed below) coexists with the $\sqrt{3}\times\sqrt{3}$ structure, and the number of Si-substitutional defects in the $\sqrt{3}\times\sqrt{3}$ regions continues to decrease until the entire surface consists of the $\sqrt{7}\times\sqrt{7}$ structure.

### 3. *Electronic structure of $\sqrt{3}\times\sqrt{3}$ overlayers*

In order to understand the electronic structure of the $\sqrt{3}\times\sqrt{3}$ overlayer, tunneling-spectroscopy measurements were also performed on both "ideal" and "defect"

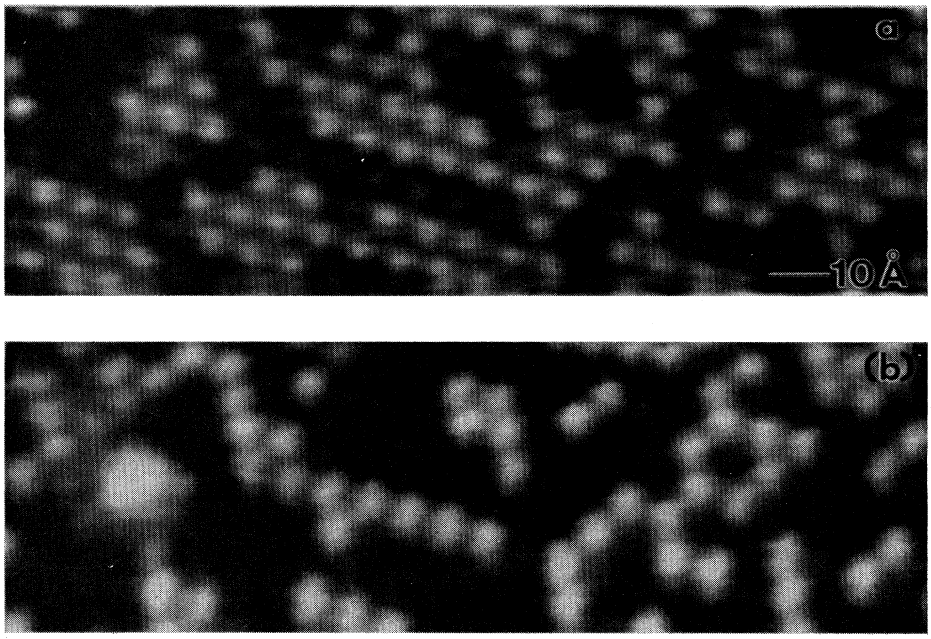


FIG. 3. STM topographic image of a single region with $\frac{1}{6}$ ML Al coverage. The local nature of the $\sqrt{3}\times\sqrt{3}$ bonding permits selective imaging of (a) Al adatoms at positive sample bias and (b) Si adatoms at negative sample bias.

structures in the $\sqrt{3}\times\sqrt{3}$ overlayer, as shown in Fig. 4. These measurements show that in defect-free regions of $(\sqrt{3}\times\sqrt{3})$Al [Fig. 4(a)] there is a pronounced surface-state band gap, with the density of states first increasing near $-0.3$ and $+0.5$ eV. Peaks in the tunneling DOS measurements are observed at energies of $+0.9$ and $\simeq -1.5$ eV. In order to ensure that these states were characteristic of the *sample* rather than the tip, similar measurements were performed on evaporated Al films. Tunneling-spectroscopy measurements on those films with the same tips showed relatively featureless *I-V* profiles with no evidence for surface-state band gaps. Thus, the band gap observed for the $\sqrt{3}\times\sqrt{3}$ overlayer must be intrinsic to the $\sqrt{3}\times\sqrt{3}$ overlayer and not predominantly associated with the electronic structure of the tip.

For comparison, Fig. 4(c) shows the predicted structure for $(\sqrt{3}\times\sqrt{3})$Al/Si(111) calculated by Northrup[1] together with the results of experimental band-structure measurements by Nicholls *et al.*[17] The tunneling-spectroscopy measurements are in agreement with the experimental results for both occupied and unoccupied states. A comparison with Northrup's calculation[1] shows that the experimental band gap is somewhat larger than that predicted, but the dispersions of the individual bands are in good agreement.

Tunneling-spectroscopy measurements were also made at the isolated Si substitutional defects at Al coverages near $\frac{1}{3}$ ML, where the density of defects is relatively low [Fig. 4(b)]. Under these conditions, the distance between defects is considerably greater than the electrostatic screening length, so the defects are essentially isolated from one another. As shown in Fig. 4(b), the quantity

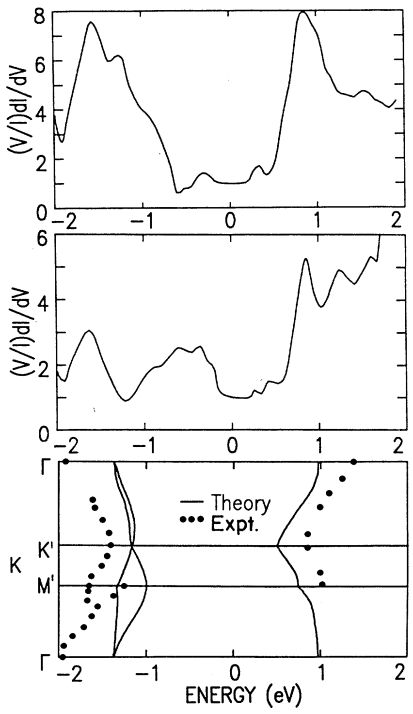


FIG. 4. Tunneling-spectroscopy measurements for Si(111)-$(\sqrt{3}\times\sqrt{3})$Al: (a) spectroscopy data obtained on "ideal" region of $(\sqrt{3}\times\sqrt{3})$Al, (b) spectroscopy data obtained over Si-substitutional defect, and (c) calculated surface band structure (from Ref. 1) and experimental photoemission results (from Ref. 17) for $(\sqrt{3}\times\sqrt{3})$Al.

$(V/I)(dI/dV)$ at these isolated defects has a broad maximum near $-0.4$ eV and a minimum near $E_F$. An electronic state at this energy has also been observed in previous ultraviolet-photoemission-spectroscopy (UPS) experiments.[11,13] Kinoshita *et al.*[11] showed UPS spectra as a function of coverage under preparation conditions nearly identical to those utilized here. The coverage-dependent measurements of the density of Si-substitutional defects obtained by STM closely correspond to the coverage dependence of the intensity of the $-0.4$-eV photoemission feature, strongly suggesting that they arise from the same defect structures. Surprisingly, measurements of the apparent "height" of the Al adatoms adjacent to these defects shows that they are apparently unaffected by the defect. This insensitivity of the $\sqrt{3}\times\sqrt{3}$ adatoms to the chemical identity of their neighbors likely results from the relatively large separation of the adatoms in the $\sqrt{3}\times\sqrt{3}$ structure (6.66 Å). The STM measurements consistently indicate that the adatom structures, both for the $(\sqrt{3}\times\sqrt{3})$Al overlayer and for the Si-substitutional defects, are characterized by very *localized* electronic states. The localized nature of these Si-substitutional defects has been addressed in more detail in a previous publication,[18] and is consistent with angle-resolved-photoemission measurements,[11,13] which show that the $-0.4$-eV "defect" state in photoemission has less than 0.1 eV dispersion across the entire surface Brillouin zone.

#### 4. *Bonding and electronic structure of Si(111)-$(\sqrt{3}\times\sqrt{3})$Al*

The Si(111)-$(\sqrt{3}\times\sqrt{3})$ structure has been widely studied using LEED,[5,15] UPS,[11–13,19] inverse-photoemission[17] spectroscopy, and electron-energy-loss spectroscopy.[15] Theoretical calculations of the electronic and geometric structure have likewise been performed for the $\sqrt{3}\times\sqrt{3}$ structure.[1,2,14]

At $\frac{1}{3}$ ML Al coverage the most natural model for the $\sqrt{3}\times\sqrt{3}$ overlayer is a simple adatom structure in which Al atoms adsorb atop a bulklike Si(111) lattice. In this model, each Al adatom saturates three Si dangling bonds. By arranging the Al adatoms in a $\sqrt{3}\times\sqrt{3}$ geometry, complete saturation of all silicon dangling bonds is achieved at $\frac{1}{3}$ ML Al.

The basic features of the Al-adatom structure are clearly supported by the STM results. The STM topographic height measurements show that at individual and small clusters of vacancy defects the tip moves $\simeq 1.5$ Å toward the surface, which is significantly smaller than the 3.1-Å step height on Si(111). This indicates that another layer of atoms is present $\simeq 1.5$ Å lower than the topmost layer of atoms, in agreement with the atomic geometry predicted from total-energy–minimization calculations[1] for adatom models. The height difference observed in STM is likely to be larger than the true geometric height difference due to the strongly localized nature of the Al unoccupied states. Further evidence is provided by images showing coexisting $\sqrt{3}\times\sqrt{3}$ and $(2\times1)$ structures, which will be discussed later. Those images show that under certain conditions the $\sqrt{3}\times\sqrt{3}$ structure can coexist with a $(2\times1)$ structure, which we believe to be a reconstruction of the *clean* Si(111) surface.[20] The $\sqrt{3}\times\sqrt{3}$ overlayer is observed to be $\simeq 1.5$ Å higher than the $(2\times1)$ structure, which is also consistent with the $\sqrt{3}\times\sqrt{3}$ structure originating from Al adatoms situated *above* the Si(111) outer double layer.

From the STM images alone, it is not possible to distinguish between the two adatom models proposed for this structure. Lander and Morrison[5] originally proposed an adatom model in which the Al atoms sit in the threefold sites with no second-layer Si atom underneath (the $H_3$ site). An alternative bonding geometry has the Al adatoms bonded to three first-layer Si atoms and also located directly above a fourth Si atom in the second atomic layer, known as the $T_4$ geometry. On the basis of total-energy calculations he performed for both the $H_3$ site and the $T_4$ site, Northrup[1] has predicted that the $T_4$ site should be more stable by 0.3 eV/adatom and should therefore constitute the equilibrium bonding geometry.

The large energy difference between $T_4$ and $H_3$ structures indicates that the surface should consist essentially entirely of Al adatoms in the $T_4$ geometry. In their LEED work, however, Lander and Morrison[5] reported *two* different $\sqrt{3}\times\sqrt{3}$ structures depending on sample-preparation conditions. STM topographs at $(\sqrt{3}\times\sqrt{3})$-$(\sqrt{3}\times\sqrt{3})$ domain boundaries indicate that only one bonding site exists, but are by themselves unable to determine which of these two geometries is correct.

The tunneling-spectroscopy results[16] as well as photoemission results[13,17] favor the $T_4$ site over the $H_3$ site. This preference is based on Northrup's calculations,[1] which predict a band gap of $\simeq 1.5$ eV for the $T_4$ model, but only $\simeq 0.8$ eV for the $H_3$ model. The band gap observed by tunneling-spectroscopy and photoemission measurements[12,17] of nearly 2 eV is significantly larger than Northrup's predictions for either model, but are closer to the predictions for the $T_4$ model. Additional support for the $T_4$ model is provided by experimental measurements of the band dispersions for both occupied[13] and unoccupied[17] states, which show excellent agreement with the $T_4$ model but poor agreement with the $H_3$ model. Thus, it appears likely that the $T_4$ site is the correct adsorption site for the Al adatoms.

While the theoretical calculations do not accurately predict the exact energies of the surface states of Al on Si(111), they do reveal much about the character and spatial extent of the wave functions of these states, which are quite similar for both $H_3$ and $T_4$ geometries. The origin of the occupied and unoccupied electronic states for $(\sqrt{3}\times\sqrt{3})$-adatom structures has been treated in detail in several independent studies.[2,21,22] Since Al is located in group III of the Periodic Table, its most stable bonding geometry in most chemical compounds is a trigonal planar configuration. There, the threefold coordination is best described as an $sp^2$ hybridization, with an empty $p_z$ orbital perpendicular to the plane. Northrup[21] and Nagayoshi[2] have shown that a similar situation applies for Al adsorbed on threefold sites on a Si(111) surface, although here the geometry makes the hybridization intermediate between $sp^2$ and $sp^3$. The net result is that the unoccupied surface state is essentially an empty Al $3p_z$

orbital localized directly above the Al adatom, perhaps with some contributions from the 3*s* state. In contrast, these same calculations show that the occupied states are formed from the $p_x$ and $p_y$ orbitals of the Al adatom interacting with the $p_z$-like "dangling bonds" of the Si(111) surface. The resulting electronic states have their state density concentrated between the Si(111) plane and the Al adatom. Nagayoshi's calculations[2] show that this maximum in the occupied state density lies almost directly above the first-layer Si atoms.

The STM images clearly reflect these pronounced differences in the spatial location and degree of localization of occupied and unoccupied states. Large corrugations are observed in the STM images at positive sample bias, as here the tip essentially follows the contours of the $p_z$-like empty state centered on the Al adatoms. The protrusions observed under these conditions then accurately reflect the positions of the Al adatoms.

When tunneling out of the occupied surface states, however, the interpretation is not as straightforward. Bias-dependent STM images as well as local tunneling *I-V* measurements show that the protrusions observed at positive and negative bias are laterally coincident. Yet, calculations by Nagayoshi[2] predict that the occupied-state density is highest directly above the first-layer Si atoms, whereas the unoccupied-state density is highest above the Al adatoms. On the basis of these calculations, one might have expected to see a lateral shift between positive- and negative-bias STM images. The shift between negative- and positive-bias STM images anticipated from these calculations is absent primarily because, while electronic-structure calculations generally calculate the state density near the surface plane, STM measurements are performed with a tip located 8–10 Å away from the surface plane and, therefore, they only sense the *tails* of these wave functions. For example, recent calculations show[2,22] that while the density of occupied states reaches its absolute maximum close to the Si atoms, planar cuts taken further from the surface show their maximum directly above the Al adatoms, in agreement with the STM results. This indicates that considerable care must be taken when comparing electronic-structure calculations with STM results.

The tunneling-spectroscopy and bias-dependent STM-topography results, in conjunction with the theoretical calculations, demonstrate that the unoccupied Al adatom states are $p_z$-like in nature, giving rise to large corrugations which can be directly associated with the positions of the Al adatoms. For the occupied states, however, the relation between the STM images and the surface geometric structure is complicated because the occupied surface states are localized between the Al adatom and the Si surface, and so do not exhibit a simple exponential decay into the vacuum. This kind of complicated spatial dependence of occupied states is expected to widely occur for many other types of simple adatom structures as well, since the energetics of bonding usually require that occupied bonding electronic states be localized on a plane lying between the adatoms and the substrate, rather than on the vacuum side of the adatoms. In the case of aluminum on silicon, simple electronegativity considerations indicate (and experimental measurements verify) that charge transfer is primarily from Al to Si. As a result, it is expected[23] that the positions of the Al adatoms are likely to be revealed in positive-bias STM images.

### B. Si(111)-($\sqrt{7}\times\sqrt{7}$)*R* 19.1°-Al

#### *1. Tunneling-microscopy and -spectroscopy results*

When the Al coverage is increased above $\frac{1}{3}$ ML, regions having ($\sqrt{7}\times\sqrt{7}$)*R* 19.1° symmetry are observed in the STM images. Figure 5 shows STM images of this structure. At positive sample bias (sampling empty surface states), STM images reveal three protrusions per $\sqrt{7}\times\sqrt{7}$ unit cell, forming an equilateral triangle with maxima 5.4 Å ($\simeq 1.4a$, where $a=3.84$ Å) apart. Voltage-dependent STM imaging shows that all three protrusions have the same height irrespective of the bias voltage in the accessible range between 1.0 and 2.5 V. The absence of voltage-dependent variations in the relative heights indicates that the three protrusions arise from electronically, and hence structurally, equivalent structures. STM images acquired at negative bias [Fig. 5(b)] are strikingly different, revealing only a *single* protrusion in each unit cell. The pronounced difference between negative- and positive-bias images demonstrates a wide spatial separation of filled and empty surface states.

The energies of these filled and empty states have been determined from tunneling-spectroscopy measurements in $\sqrt{7}\times\sqrt{7}$ regions, as shown in Fig. 5(c). These measurements show that the $\sqrt{7}\times\sqrt{3}$ structure, like the $\sqrt{3}\times\sqrt{3}$ structure, shows a large surface state band gap. At energies between $\simeq -0.2$ and $+0.5$ eV, the density of states is so low that no tunneling data could be obtained. Peaks in the $\sqrt{7}\times\sqrt{3}$ state density are observed in tunneling measurements near $-0.7$ and $+1.0$ eV. A more detailed comparison between the electronic structures of the $\sqrt{3}\times\sqrt{3}$ and $\sqrt{7}\times\sqrt{3}$ overlayers is also possible because of the frequent occurrence of sharp boundaries between $\sqrt{3}\times\sqrt{3}$ and $\sqrt{7}\times\sqrt{7}$ structures, which will be discussed in more detail below. Tunneling *I-V* curves were measured at each location while scanning across regions which included boundaries between $\sqrt{3}\times\sqrt{3}$ and $\sqrt{7}\times\sqrt{7}$ structures. Under these conditions the electronic structure of the tip is assured to be the same on each side of the boundary, thereby permitting a direct comparison of their tunneling *I-V* characteristics of the $\sqrt{3}\times\sqrt{3}$ and $\sqrt{7}\times\sqrt{7}$ overlayers on each side. Those measurements confirm that the energy of the unoccupied state is quite similar to that of the $p_z$-like state of the $\sqrt{3}\times\sqrt{3}$ structure, while the occupied states of the $\sqrt{7}\times\sqrt{7}$ overlayer are approximately 0.3 eV closer to the Fermi level than those for ($\sqrt{3}\times\sqrt{3}$) Al. A similar upward shift in the energy of the occupied states of the $\sqrt{7}\times\sqrt{7}$ structure has been observed in UPS measurements by Kinoshita *et al.*[11] The existence of a surface-state band gap on this surface is further supported by our earlier observation of strong local band-bending effects around vacancy defects on this surface.[24] Thus, even at $\frac{3}{7}$ ML coverage the states associated with Al—Si bonding

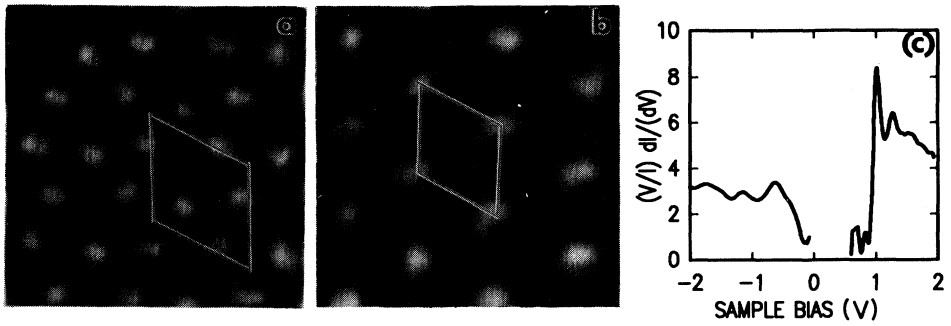


FIG. 5. Constant-current topographs of Si(111)-($\sqrt{7}\times\sqrt{7}$)$R$ 19.1° structure at positive [(a), +1.6 V)] and negative [(b), −1.6 V] bias, and results of tunneling-spectroscopy measurements [(c)].

do not provide a significant density of states of $E_F$, and so cannot pin the Fermi level.

### 2. *Boundaries with other ordered overlayers*

The $\sqrt{7}\times\sqrt{7}$ and $\sqrt{3}\times\sqrt{3}$ structures coexist in close proximity, so that domain boundaries between the two often can be observed. Although the boundaries are often irregular and do not appear to follow the surface crystallographic directions, the transition from $\sqrt{3}\times\sqrt{3}$ to $\sqrt{7}\times\sqrt{7}$ is usually very sharp, with very little disorder on either side of the boundary. Figure 6 shows such a boundary between $\sqrt{3}\times\sqrt{3}$ and $\sqrt{7}\times\sqrt{7}$ structures, acquired with a ~1.6-V sample bias. Here, the $\sqrt{3}\times\sqrt{3}$ structure appears in the central region, with the $\sqrt{7}\times\sqrt{7}$ structure appearing on the left and right sides. It is apparent that both the $\sqrt{3}\times\sqrt{3}$ and $\sqrt{7}\times\sqrt{7}$ overlayers are quite perfect even very near the ($\sqrt{3}\times\sqrt{3}$)-($\sqrt{7}\times\sqrt{7}$) boundary.

These boundaries prove extremely useful in developing an atomic model for this unknown overlayer structure. The lattice vectors of the $\sqrt{7}\times\sqrt{7}$ overlayer are rotated 19.1° with respect to the [1$\bar{1}$0] lattice vector, which joins nearest-neighbor Si atoms on the bulk-terminated (111) surface. The +19.1° and −19.1° domains are rotationally inequivalent, but are related by reflection through a [1$\bar{1}$0] mirror plane.

In order to develop a model for the $\sqrt{7}\times\sqrt{7}$ structure

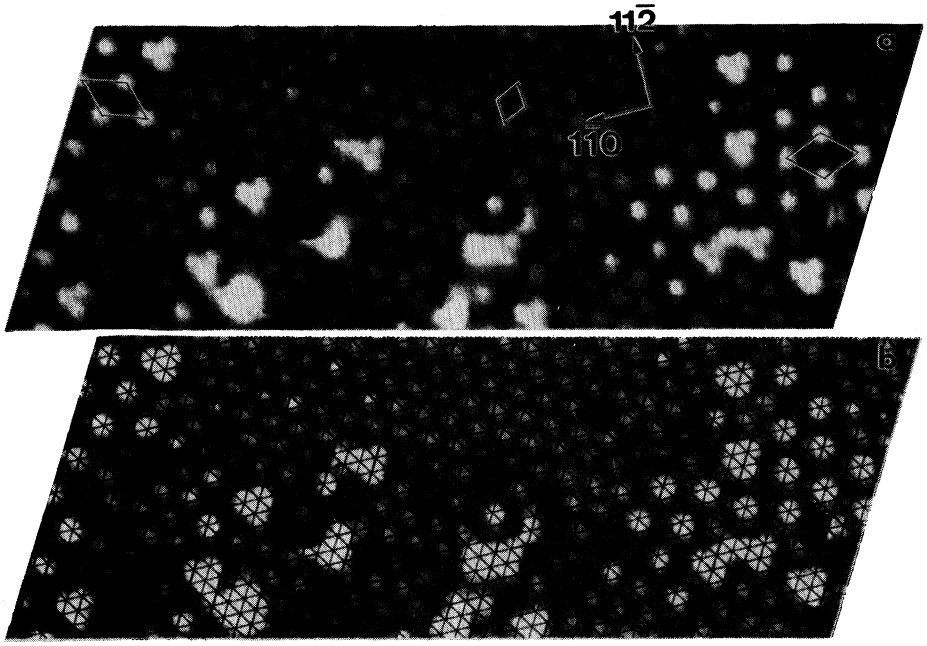


FIG. 6. domain boundary between $\sqrt{3}\times\sqrt{3}$ (center) and $\sqrt{7}\times\sqrt{7}$ (left and right) structures, obtained at sample bias of −1.6 eV.

from the STM images, it is necessary to first determine the rotational orientation of each domain as $+19.1°$ or $-19.1°$ with respect to the $[1\bar{1}0]$ direction of the underlying Si(111) lattice. In general, thermal drift and creep of the piezoelectric scanners in the STM makes it difficult to determine crystallographic orientations with good accuracy. However, in images which include $(\sqrt{7}\times\sqrt{7})$-$(\sqrt{3}\times\sqrt{3})$ domain boundaries, the $\sqrt{3}\times\sqrt{3}$ structure can be used to accurately establish the surface crystallographic orientation *in situ,* since the real-space basis vectors of the $\sqrt{3}\times\sqrt{3}$ overlayer are rotated 30° with respect to $[1\bar{1}0]$ and the $+30°$ and $-30°$ orientations are equivalent. This procedure then allows the absolute rotational orientation of the $\sqrt{7}\times\sqrt{7}$ unit cells ($+19.1°$ or $-19.1°$) to be established. In Fig. 6 both these orientations are observed.

Similarly, the existence of sharp boundaries between $\sqrt{3}\times\sqrt{3}$ and $\sqrt{7}\times\sqrt{7}$ overlayers allows the relative *translational* orientation of the overlayers to be established. This is achieved by fitting the $\sqrt{3}\times\sqrt{3}$ region to a hexagonal lattice and then extrapolating the lattice a short distance across the boundary into the $\sqrt{7}\times\sqrt{7}$ region. This lattice-extrapolation technique is particularly straightforward here, since the results presented above demonstrate that the protrusions observed for the $\sqrt{3}\times\sqrt{3}$ structure are essentially bias independent and represent the positions of the Al adatoms on $T_4$ or (possibly) $H_3$ sites.

The results of this fitting procedure are shown in Fig. 6(b), where the STM image in Fig. 6(a) is reproduced, but now with a hexagonal lattice superimposed. The translational and rotational orientations of the lattice were adjusted to optimize the fit in the $\sqrt{3}\times\sqrt{3}$ region; the $\sqrt{3}\times\sqrt{3}$ protrusions were centered in the open triangles of the lattice to represent threefold sites. The resulting fit shows that the protrusions in the negative-bias $\sqrt{7}\times\sqrt{7}$ region are displaced by $4a_0/3\sqrt{2}$ along the $[11\bar{2}]$ direction relative to the protrusions in the $\sqrt{3}\times\sqrt{3}$ region. If the $T_4$ model for the $\sqrt{3}\times\sqrt{3}$ overlayer is assumed to be correct, then this domain-boundary result establishes that the single protrusion observed at negative sample bias for the $\sqrt{7}\times\sqrt{7}$ overlayer is located at an on-top site.

Figure 7 shows a similar domain-boundary image taken at *positive* sample bias, where the characteristic trimers are observed in the $\sqrt{7}\times\sqrt{7}$ region. Again, the $\sqrt{3}\times\sqrt{3}$ structure is used to determine the absolute rotational orientation of the $\sqrt{7}\times\sqrt{7}$ domain, which here is 19.1° with respect to $[1\bar{1}0]$. From these boundary-domain images it can be established that lines connecting pairs of atoms in each trimer are rotated $\simeq 15°$ with respect to the $[1\bar{1}0]$ family of lattice directions. Applying the lattice-extrapolation technique described above to this and other similar images indicates that the positions of these protrusions correspond to twofold sites of the bulk-terminated (111) lattice.

The relative orientation of the images at positive and negative bias is further established by topographic scans taken at positive and negative bias over identical regions, using point defects to achieve registration between the images. These images show that the "dangling bond" observed at negative sample bias originates in the same location as the deep depressions between the trimers observed at positive sample bias.

### 3. *Structural model for Si(111)-$(\sqrt{7}\times\sqrt{7})R19.1°$-Al*

In order to develop an improved structural model from the STM images, it is necessary to understand how the surface geometry relates to the position and energies of all the electronic states. In the previous case of $(\sqrt{3}\times\sqrt{3})$Al, it was shown that Al adsorption onto Si(111) is accompanied by a substantial redistribution of electron density in order to form the necessary bonding orbitals. Since the bonding orbitals are localized between the Al adatom and the Si(111) surface, there is a decreased electron density (or a higher density of unoccupied surface states) on the vacuum side of the Al adatom. As a result, the *unoccupied* surface states were shown to be representative of the Al-adatom positions in the $\sqrt{3}\times\sqrt{3}$ structure. Although detailed electronic-structure calculations will ultimately be required to fully understand the electronic structure of the other overlayers formed by Al on Si(111), a similar spatial redistribution of charge between an Al adatom and a Si(111) substrate should also occur for other types of simple adatom structures. Thus, for Al-adatom structures it is expected

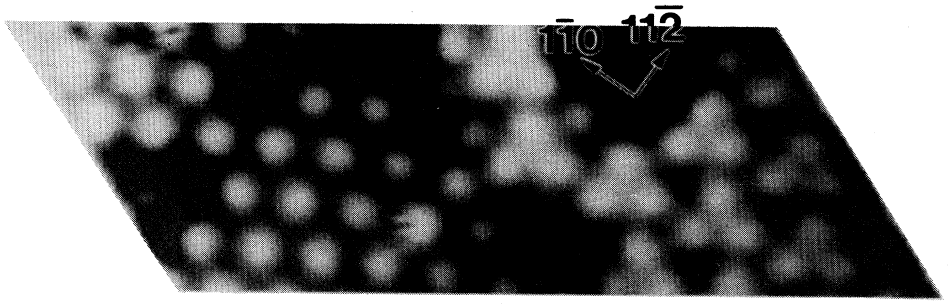


FIG. 7. Domain boundary between $\sqrt{3}\times\sqrt{3}$ (left) and $\sqrt{7}\times\sqrt{7}$ (right) structures, obtained at sample bias of $+1.6$ eV. Crystallographic orientations are given.

that STM images probing the *unoccupied* states of the sample are most likely to provide information about the adatom geometric positions.

Applying these arguments to the $\sqrt{7}\times\sqrt{7}$ overlayer indicates that there are three Al adatoms per $\sqrt{7}\times\sqrt{7}$ unit cell. Since the bulk-truncated Si(111) surface has seven Si atoms in each $\sqrt{7}\times\sqrt{7}$ unit cell, this places the local Al coverage at $\frac{3}{7}$ (=0.43) ML. A local coverage of $\frac{3}{7}$ ML is also indicated by the tunneling-spectroscopy measurements and the following simple electron-counting argument. While an *odd* number of valence electrons would be expected to produce a half-filled (metallic) band of surface states, the large surface-state band gap observed in tunneling spectroscopy indicates that there are an *even* number of valence electrons in each unit cell. Since the bulk-truncated Si(111) surface has seven Si dangling bonds in each unit cell and the three Al adatoms contribute a total of three valence electrons from their $3p$ orbitals, a total of ten valence electrons are available for the surface-state bands in each unit cell, which is consistent with formation of a surface-state band gap. In contrast, local coverages of $\frac{2}{7}$ or $\frac{4}{7}$ ML would result in odd numbers of valence electrons and therefore would be expected to produce a half-filled metallic band at $E_F$. This $\frac{3}{7}$-ML coverage is also consistent with previous studies,[12] which have determined that the $\sqrt{7}\times\sqrt{7}$ structure arises at Al coverages between 0.25 and 0.5 ML.

Hansson[12] also noted that the existence of a large surface-state band gap implies a local coverage of $\frac{3}{7}$ ML, and used this as the basis of a structural model for this overlayer. In Hansson's model, each $\sqrt{7}\times\sqrt{7}$ unit cell contains three Al adatoms in a cluster on equivalent threefold sites, as shown in Fig. 8(a). The rotational orientation of the clusters predicted by Hansson's model, however, is inconsistent with the STM images. In Hansson's model, lines connecting pairs of protrusions within each trimer should be oriented parallel to $[1\bar{1}0]$. In contrast, the STM images show that the clusters are rotated by nearly 15°. Thus, the symmetry of the STM images appears to be inconsistent with Hansson's model. A closer look at Hansson's model reveals one major difficulty, namely that the model predicts sixfold coordination for the Si atom situated in the center of each Al trimer, while Si generally prefers fourfold coordination. Such a high coordination number for silicon seems quite unlikely.

Finding this model unsatisfactory, attempts were made to model the atomic structure using various combinations of $T_4$, $H_3$, onefold (atop), and substitutional geometries. Such combinations were also found to be unsatisfactory because they failed to reproduce the most basic features of the $\sqrt{7}\times\sqrt{7}$ surface—the clustering of the Al adatoms and their orientation of the clusters with one another. In addition, the STM results show that the three protrusions observed at positive bias appear to be electronically (and hence, structurally) equivalent.

A modification of Hansson's model, however, achieves excellent agreement with the STM measurements. The motivation for this modification is to reduce the high coordination of the central Si atom in Hansson's model. This can be achieved by displacing the Al adatoms in each cluster radially outward onto equivalent twofold sites, as in Fig. 8(b). This radial displacement moves the Al adatoms in Hansson's clusters further apart; at the same time, it moves Al adatoms from adjacent clusters closer together, in effect forming *new* sets of clusters, as shown in Fig. 8(c). Lines connecting pairs of adatoms in the new clusters are rotated by 10.9° with respect to $[1\bar{1}0]$, and the Al adatoms within each cluster are separated by $\sqrt{7}\,a/2=5.1$ Å. Both the rotational orientation and the individual-atom separations predicted by this new model are in excellent agreement with the STM measurements made at positive sample bias, under conditions where our earlier arguments indicated that STM should be imaging the positions of the Al adatoms. A second characteristic of this new model is that it predicts a lone Si "dangling bond" in each unit cell, labeled DB in Fig. 8(c), at the same location where the STM images reveal a single protrusion at negative sample bias.

In order to evaluate this model, we also consider the electronic structure expected to result from clustering of Al adatoms on twofold sites of a bulk-terminated Si(111) surface. Tunneling-spectroscopy results show that there is a pronounced surface-state band gap, so that any Si

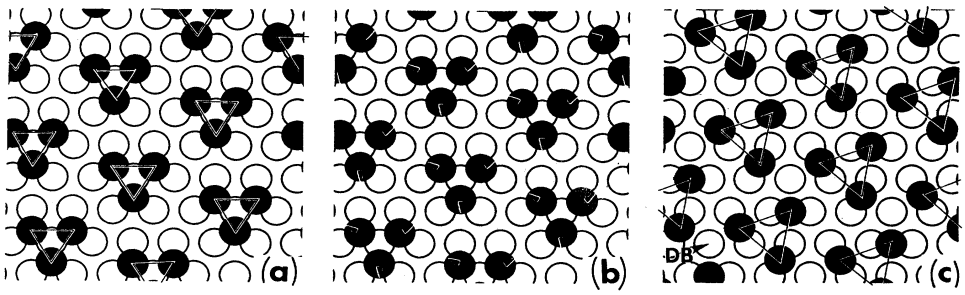


FIG. 8. Models for $(\sqrt{7}\times\sqrt{7})$ structure: (a) Hansson's model (from Ref. 12); (b) radial displacement of Al adatoms due to overcoordination of central Si atom; (c) new model for $\sqrt{3}\times\sqrt{3}$ resulting from the radial displacements of (b).

"dangling-bond" states must be completely occupied or unoccupied. Counting the $2p$ valence electrons of both Al and Si, we find that in each $\sqrt{7}\times\sqrt{7}$ unit cell there are nine valence electrons from the three Al adatoms, but only seven unpaired valence electrons distributed on the seven threefold-coordinated Si atoms (assuming a bulk-terminated structure for (Si). Thus, the number of valence electrons associated with the aluminum atoms is in excess of that required to saturate the Si dangling bonds through simple charge transfer. We propose that these extra electrons from the Al atoms change the local bonding to favor lower coordination of the Al adatoms and also completely occupy a "dangling bond" on the single threefold-coordinated Si atom remaining in each unit cell.

The manner in which this is accomplished can be understood from the experimental STM results combined with the results of recent electronic-structure calculations. Nelson and Batra[22] have recently performed electronic-structure calculations for Al trimers on twofold sites in a geometry similar to that proposed here. As for the $\sqrt{3}\times\sqrt{3}$ structure, these calculations show that the Al adatoms on the twofold sites bond strongly to their adjacent Si atoms, leading to energetically low-lying bonding states which are spatially localized between the Al adatoms and the Si substrate. In addition, however, Nelson's calculations show that the three Al adatoms and the central Si atom are also capable of forming a partially delocalized, cooperative bonding state. We propose that in the ($\sqrt{7}\times\sqrt{7}$)Al structure such a cooperative bonding state forms which involves one electron from each of the three Al adatoms and a fourth electron from the central Si "dangling bond." The total of four electrons in the cooperative bonding state effectively "fills" the Si dangling-bond state and leads to a surface-state band gap. We also expect there to be a strong $p_z$-like unoccupied state associated with each Al adatom, like that observed for the $\sqrt{3}\times\sqrt{3}$ structure.

The experimental and theoretical results therefore indicate that there are two fundamentally different types of occupied electronic states associated with the Al adatoms atop twofold sites. One is primarily associated with the direct bonding of each Al adatom at its twofold site, which the second type is a delocalized state involving the interaction of the Al adatoms with the long Si "dangling bond." STM images acquired at negative sample bias should primarily reflect the spatial distribution of the highest-energy occupied state, since the highest-energy electrons will experience the smallest tunneling barrier. The STM images at negative bias reveal a strong occupied-state density centered at the central Si atom and are in full agreement with the expected spatial distribution from this bonding geometry. This leads us to propose that the increased state density observed in tunneling spectroscopy near $-0.8$ eV arises primarily from the cooperative bonding state. The occupied electronic states associated with the Al bonding to the twofold Si atoms are likely to be lower in energy, as for the $\sqrt{3}\times\sqrt{3}$ geometry, giving rise to the state density in the regions between $-1.4$ and $-1.8$ eV. Finally, each Al adatom has with it an unoccupied state lying near 1.1 eV above $E_F$ that appears to be essentially a localized, unoccupied $sp^3$-hybridized orbital, much like that observed for the $\sqrt{3}\times\sqrt{3}$ structure. At positive sample bias, electrons tunnel into this unoccupied state on each Al adatom, revealing the characteristic clustering. The atomic geometry of this ($\sqrt{7}\times\sqrt{7}$) structure, shown in Fig. 8(c), is determined by a complex interplay between minimizing the number of "dangling" bonds, optimizing coordination of both Al and Si atoms, and minimizing interactions between adjacent Al adatoms.

### C. (2×1) structure

A structure having (2×1) symmetry has also been occasionally observed in coexistence with the $\sqrt{3}\times\sqrt{3}$ and $\sqrt{7}\times\sqrt{7}$ structures. This structure has not been reported in any previous studies of Al/Si(111), presumably because it only occupies only a small fraction of the surface and because it may require unusual preparation conditions. The (2×1) structure was observed in STM when $\simeq 0.5$ ML Al was deposited on Si(111), followed by a short anneal to $\simeq 1100$ K for 15 s. At this temperature, Al slowly evaporates from the surface. Short-time anneals produce coexisting $\sqrt{7}\times\sqrt{7}$ and $\sqrt{3}\times\sqrt{3}$ domains, while over longer time periods the aluminum is completely removed and the clean Si(111)-(7×7) structure is restored. Since the (2×1) structure was observed only infrequently, the best preparation conditions could not be determined.

The surface structures produced by this annealing procedure are shown in Fig. 9, at $-1.6$ V sample bias. This image shows *two* domains of the (2×1) structure coexisting with $\sqrt{7}\times\sqrt{7}$ (upper left corner) and $\sqrt{3}\times\sqrt{3}$ (center and upper right) structures. A corrugation profile passing through all three structures is shown in Fig. 9(b). The (2×1) structure appears to be the lowest, with the $\sqrt{3}\times\sqrt{3}$ structure $\simeq 1.5$ Å higher than the (2×1) structure. The $\sqrt{7}\times\sqrt{7}$ structure exhibits large corrugations, but its minimum height is close to the minimum height observed in the $\sqrt{3}\times\sqrt{3}$ structure. Since the double-layer step height on Si(111) is 3.1 Å, these results indicate that all three structures are associated with the same Si(111) terrace (i.e., there is no step present).

The rare occurrence of this structure and the limited amount of data obtained permit only speculations about its origin. However, the corrugation profiles are consistent with its assignment as a (2×1) reconstruction of the clean Si(111) surface. Total-energy calculations[1,20] suggest that a height difference of $\simeq 1$ Å would be expected between the outermost layer of atoms in the Si(111)-($\sqrt{3}\times\sqrt{3}$) and metastable clean Si(111)-(2×1) structures, in agreement with the height difference of $\simeq 1.5$ Å observed in Fig. 9. Additionally, the corrugation profiles taken along the two high-symmetry directions of the (2×1) structure show corrugations of $\simeq 0.6$ and 0.2 Å, in good agreement with the values reported on the (2×1) reconstruction formed by cleaving pure Si.[25]

Although Si(111)-(2×1) is normally formed by cleavage, small regions of Si(111)-(2×1) have also been previously identified via STM in Si(111) wafers which were either sputter annealed[26] or else rapidly quenched.[27]

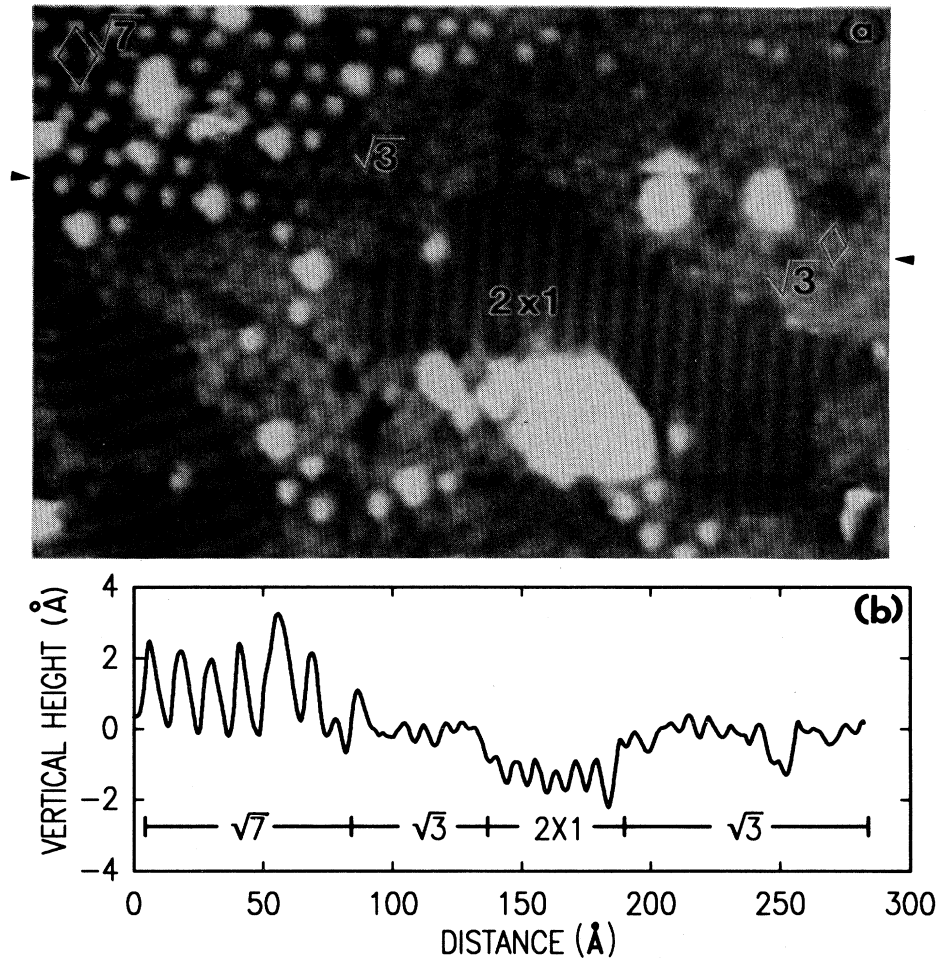


FIG. 9. (a) STM images showing two domains of (2×1) structure coexisting with ($\sqrt{3}\times\sqrt{3}$)Al [surrounding (2×1) regions] and $\sqrt{7}\times\sqrt{3}$ (top left) structures. Arrows denote starting and ending points for (b), the corrugation profile over the various superstructures observed in (a).

In the Al-overlayer experiments reported here, the (2×1) reconstruction likely arises from the rapid evaporation of aluminum to expose small, flat terraces of clean silicon. Since the (2×1)-to-(7×7) transformation on large Si(111) terraces occurs at comparatively low temperatures, the (2×1) terraces exposed by Al evaporation can only persist under the evaporation conditions if there is an unusually large activation barrier to the transformation. Upon evaporation of the Al adatoms, formation of the (7×7) structure requires both extensive atomic rearrangements in the outer surface layers and also mass transport of Si atoms from step edges along the surface plane, in order to establish the layer of Si adatoms. Thus, a relatively large kinetic activation barrier would be expected. In contrast, formation of the (2×1) structure involves only small translations of Si atoms in the outermost atomic layer, and should be kinetically favored. These ideas are supported by LEED studies which have shown that the Si(111)-($\sqrt{3}\times\sqrt{3}$)Al structure can be formed at room temperature simply by depositing $\frac{1}{3}$ ML Al onto the cleaved Si(111)-(2×1) surface,[28] while much higher temperatures are required when starting with Si(111)-(7×7). Microscopic reversibility arguments then suggest that during the reverse process, evaporation of Al from the $\sqrt{3}\times\sqrt{3}$ structure, the Si(111)-(2×1) structure might be formed as a relatively stable kinetic intermediate. The stability of the (2×1) reconstruction on these small terraces might also be increased by the absence of steps, which can act as nucleation sites for formation of the (7×7) reconstruction.[29]

### D. Si(111)-(7×7)Al

#### *1. Tunneling-microscopy and -spectroscopy results*

Above $\frac{3}{7}$ ML coverage, a new overlayer with (7×7) symmetry is observed. Our coverage-dependence measurements are in agreement with the LEED data,[5,30] which find the (7×7) overlayer at Al coverages between 0.5 and 1 ML. STM images of this Si(111)-(7×7)Al overlayer at positive sample bias [Fig. 10(a)] show an irregular arrangement of triangle-shaped structures. Although the

triangles have slightly irregular sizes and shapes, there is a clear tendency for the edges of the triangular regions to be aligned along the principal (111)-surface lattice directions. Despite the fact that the (7×7)Al overlayer exhibits poor short-range order, the existence of good long-range order is clearly demonstrated in Fig. 10(b), which shows the two-dimensional fast Fourier transform (2D FFT) of this topograph. Well-defined spots are clearly observed in the 2D FFT, demonstrating that the triangular regions have a well-defined *average* edge length, giving rise to a new surface basis vector.

In order to determine the periodicity of this structure with STM, the piezoelectric transducers were calibrated after evaporating the aluminum at high temperature to recover the clean Si(111)-(7×7) surface. STM images were then obtained over an area with the same dimensions as the images of the (7×7)Al overlayer, and the STM images of the clean Si(111)-(7×7) surface and the Al-induced (7×7) overlayer were analyzed using 2D FFT technique. Possible effects of drift and piezoelectric creep were minimized by relatively rapid scanning, by measuring distances parallel to the fast-scan direction, and by proper application of drift-correction techniques when necessary. From these measurements the real-space lattice constant of the Al-induced (7×7)-overlayer constant was determined to be $(6.9\pm0.2)a_0$.

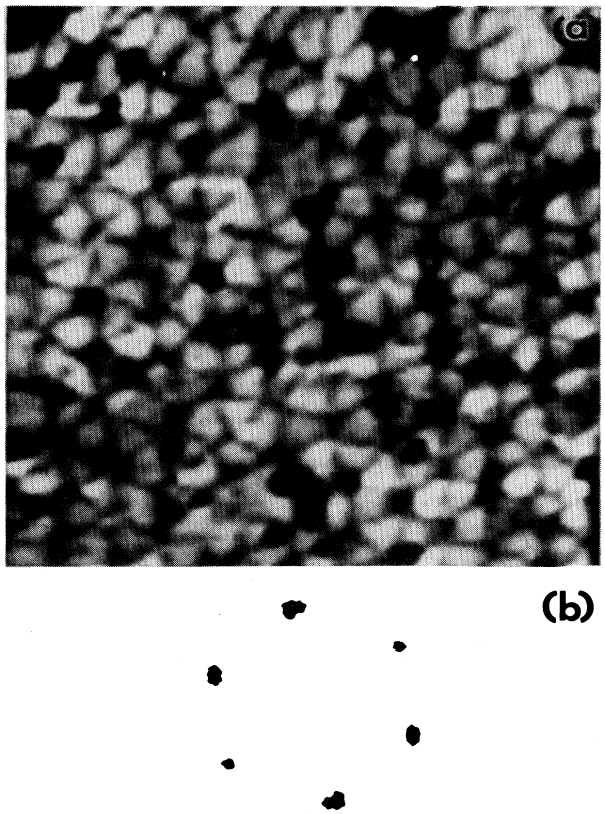


FIG. 10. Tunneling results for Si(111)-(7×7)Al structure at 1 ML coverage: (a) large-area scan, +1.5 eV sample bias; (b) two-dimensional fast Fourier transform of image shown in (a).

Figure 11 shows an image of a smaller area, again at positive bias. Here it can be seen that the triangular regions are not flat, but appear to be somewhat "puckered." The triangles are separated by jagged troughs approximately 0.4 Å deep. No significant structure is observed within the islands, although at the intersections of the triangles [which are reminiscent of the "corner holes" of the Si(111)-(7×7) surface] smaller irregular features can often be observed. Defects consisting of bright protrusions (labeled *D* in Fig. 11) are sometimes observed, almost always at the corner holes. The existence of these features and their reproducibility in repeated scans over the same area indicate that the lack of structure within the triangular subunits does not arise from a "dull tip," but instead results from a spatial delocalization of the electronic states of the high-coverage (7×7)Al structure.

On images encompassing large areas, the triangles pointing along $\langle 11\bar{2}\rangle$ and $\langle \bar{1}\,\bar{1}\,2\rangle$ directions appear to be nearly equivalent (on the average) at all bias voltages. In small regions, differences are sometimes observed between oppositely directed triangles, but these differences are not consistent from area to area. This indicates that the periodicity of the Al (7×7) structure is unrelated to the (7×7) periodicity of the clean Si(111) surface, where

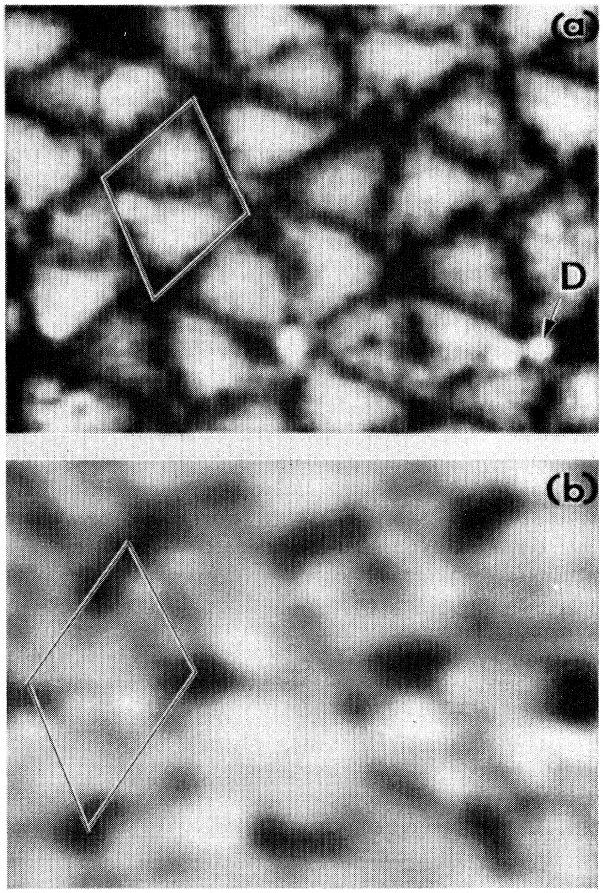


FIG. 11. High-resolution STM topographs of Si(111)-(7×7)Al: (a) high-resolution scan, +1.5 eV sample bias; (b) high-resolution scan, −1.2 eV sample bias.

changes in the stacking sequence create electronic-structure differences which are manifested as apparent height differences between oppositely directed triangles under some biasing conditions. This conclusion is further supported by the general irregularity of the unit-cell boundaries in the Al (7×7) structure; the alternating stacking sequence of the dimer–adam–stacking-fault model for Si(111)-(7×7) does not permit such ragged boundaries.

While the triangle-shaped islands have some structure when imaged at positive sample bias, Fig. 11(d) shows the images obtained at negative sample bias are extremely flat (0.2 Å total corrugation). The troughs which marked the edges of the triangular islands at positive bias are no longer observed at negative bias, but the depressions at the intersections of the troughs are retained.

The minimal atomic structure observed for this overlayer makes a structural determination difficult from the STM images alone. However, further information can be obtained from tunneling-spectroscopy measurements. As shown in Fig. 12(a), these measurements show that the (7×7) structure is characterized by a strong unoccupied state at +1.2 eV and weak occupied states near −0.6 and −1.8 eV. Even though the STM images show that this surface possesses poor long-range order, the tunneling-spectroscopy measurements show little variation across the surface, even at the "corner holes." The only noticeable spatial variation occurs at the small $D$ defects, which appear to be more metallic than the more perfect regions of (7×7)Al. This indicates that the local electronic-structure measurements are not strongly affected by the residual disorder.

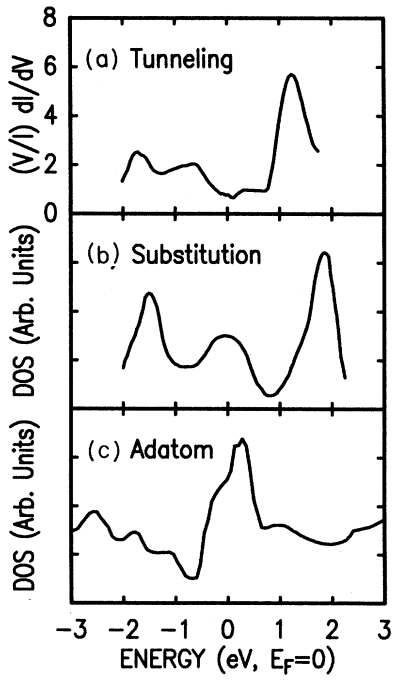


FIG. 12. (a) Tunneling-spectroscopy results for Si(111)-(7×7)Al structure, (b) density of states predicted by Chelikowsky for Al-substitution model (from Ref. 3), and (c) density of states predicted by Zhang and Schlüter for Al-adatom model (from Ref. 4).

### 2. *Atomic geometry of the (7×7) structure*

At ≃1 ML Al coverage, the most likely locations for the Al atoms are either substituting for all Si atoms in the outermost atomic layer (as proposed by Lander[5]) or as adatoms directly above the Si atoms of the outermost double layer. In transmission-electron-microscopy studies of thick films of epitaxial Al(111) on Si(111), both types of interface termination have been observed.[31] At 1 ML Al coverage, both the substitutional and the adatom models achieve saturation of all Si dangling bonds, but only Lander's substitutional model also allows the Al atoms to be threefold coordinated. Both these models have been developed assuming that the symmetry of the full monolayer structure is (1×1), not (7×7), but the relatively small spatial variations in the tunneling $I$-$V$ curves and the irregular boundaries suggest that the electronic structure is not strongly affected by the surface symmetry. For comparison, the tunneling-spectroscopy data acquired on this overlayer [Fig. 12(a)] can be compared with theoretical density-of-states calculations by Chelikowsky[3] for Lander's substitutional model [Fig. 12(b)] and with calculations by Zhang and Schlüter[4] for the on-top model [Fig. 12(c)]. The relative intensities and positions of the tunneling-spectroscopy results agree very well with Chelikowsky's calculations provided the energy scale of the later is shifted downward by ≃0.5 eV. In contrast, Fig. 12(c) shows that equivalent calculations for a onefold adatom geometry[7] are in quite poor agreement with the experiment. The tunneling-spectroscopy data, then, indicates that at coverages of ≃1 ML the Al most likely substitutes for the Si atoms in the outermost atomic layer of the Si(111) lattice. The tunneling-spectroscopy results also indicate that the (7×7)Al overlayer has a higher density of states near $E_F$ than the $\sqrt{3}\times\sqrt{3}$ or $\sqrt{7}\times\sqrt{7}$ overlayer, which results from the tail of the −0.6-eV peak extending through the Fermi energy.

The origin of the (7×7) periodicity and the detailed atomic arrangement at the boundaries of the triangular regions remains uncertain. The (7×7) periodicity here appears to be unrelated to the (7×7) periodicity of the clean surface. On the Al-covered surface oppositely directed triangles appear to be equivalent at all bias voltages, suggesting that the (7×7) periodicity does not arise from an alternating-stacking-fault structure as it does on the clean Si(111)-(7×7) surface. Instead, it probably arises from strain. Since Al is normally $sp^2$ hybridized, the lowest-energy bonding configuration likely has the Al almost coplanar with the second-layer Si atoms, distorting the Si lattice from its normal tetrahedral geometry. The presence of occasional vacancies or surface dislocations to relieve this strain could produce the dark lines observed in Fig. 10(c).

This interpretation of strain-induced overlayer symmetry is supported by transmission-electron-microscopy

studies[31] of thick films of Al on Si(111), which show that although a large (30%) lattice mismatch exists between Si(111) and Al(111), epitaxial growth still occurs because the lattice constants are close to a ratio of small integers, (here, 4 Al:3 Si).[32] The epitaxial films, however, contain a high density of dislocations at the interface, which provide a means of relieving strain. We proposed that the "troughs" and "corner holes" observed in the STM work also result from local lattice dislocations or vacancies which provide a means of relieving strain induced by the Al substitution.

It should also be noted that many of the features reported here for the (7×7) overlayer of Al/Si(111) are similar to those observed for the Cu "5×5" overlayer on Si(111), which also occurs near monolayer coverage. Recent STM results for Cu/Si(111) (Ref. 33) also show a pattern of irregularly shaped triangular tiles which give rise to an overall period of $\simeq 5.5a_0$ despite the absence of short-range order. Such strain-related reconstructions near monolayer coverage for metals on Si may be a rather general phenomenon.

## IV. DISCUSSION

These results shed considerable light on the metallization process and whether the states responsible for Fermi-level pinning are the "intrinsic" surface states (as proposed by Bardeen) or whether they are extrinsic metal-induced states lying in the gap (as proposed by Heine). Much debate has centered on the nature of the electronic states which determine the Schottky-barrier height and the surface Fermi-level position. Here, we have demonstrated the nature of the atomic rearrangements which accompany this metallization process.

At low coverage the $(\sqrt{3}\times\sqrt{3})$Al structure clearly leads to a semiconducting surface with a large gap, as the Al adatoms eliminate the midgap states originating on the Si "dangling bonds." The only states remaining near midgap are those arising from the Si-substitutional defects. While these defects show a peak DOS near $-0.4$ eV, the spectral width of this peak is clearly sufficient to provide considerable state density near $E_F$. As a result, the Si-substitutional defects pin the Fermi-level position on the $(\sqrt{3}\times\sqrt{3})$Al surface.

The ideal $\sqrt{3}\times\sqrt{3}$ structure may be regarded as a perfectly terminated Si(111) surface. When the Al coverage is increased beyond $\frac{1}{3}$ ML, the number of Al adatoms is *more* than sufficient to terminate all the Si dangling bonds. At these higher coverages, the saturation of the Si dangling bonds, which appears to be a driving force for the reconstruction of Si(111)-(7×7) and Si(111)-$(\sqrt{3}\times\sqrt{3})$Al surfaces, becomes less important, and adatom-adatom interactions become increasingly important.

One characteristic feature of the $T_4$ site for the $\sqrt{3}\times\sqrt{3}$ overlayer is the charge transfer from Al to Si, establishing a surface dipole layer. One explanation for the changes in the Al bonding site with coverage is that as the surface coverage is increased beyond $\frac{1}{3}$ ML, repulsive dipole-dipole interactions become important, and it becomes energetically favorable to *reduce* the Al-Si charge transfer. The charge transfer may be reduced in several ways. Under conditions where the Al adatom is constrained to remain bonded at the $T_4$ site, Nelson and Batra[22] have calculated that for $\Theta > \frac{1}{3}$ ML the necessary reduction in charge transfer is accompanied by an increased Al—Si bond length and a broadening of the Al-Si potential function. In reality, the Al adsorption site is *not* constrained, so that reduced Al-Si charge transfer can also be accomplished by a change in the bonding-site symmetry. The STM results here show that this is the case, as the bonding-site symmetry shifts from the $T_4$ site to twofold sites when the coverage is increased from $\frac{1}{3}$ to $\frac{3}{7}$ ML Al. Adopting the twofold site also allows for significant covalent bonding between the Al adatoms themselves, resulting in additional partially delocalized bonding states between three Al adatoms and the long Si dangling bond in each $\sqrt{7}\times\sqrt{7}$ unit cell. Although this cooperative bonding state is somewhat more delocalized than the direct Al—Si bonding states, it is not truly metallic since it is still limited in spatial extent. In fact, our earlier STM measurements around defects in the $\sqrt{7}\times\sqrt{7}$ overlayer[16] show pronounced local band-bending effects, clearly demonstrating that the density of states near $E_F$ is low for the $\sqrt{7}\times\sqrt{7}$ overlayer.

It is only at the highest coverage, and in the coincident formation of the (7×7)Al overlayer, that metallic character is observed. This is also true in room-temperature deposition, where Kelly *et al.*[34] have shown, using electron-energy-loss spectroscopy, that at low temperatures deposition of Al onto Si(111)-(7×7) results in Schottky-barrier formation which correlates with the onset of metallic character near 1 ML Al coverage. The metallic character is also evident from the very small amplitude of the STM corrugations probing both empty and filled states, since the accompanying delocalization of the wave functions reduces the local corrugation amplitude over the individual atoms (which are no longer observed).

Surprisingly, both the nature and the energy of the unoccupied electronic states appear to be little influenced by the Al coverage. The tunneling-spectroscopy measurements reported here show that all three ordered overlayers give rise to a pronounced unoccupied Al-derived state near 1.0 eV above $E_F$. This is also predicted in a number of theoretical calculations for the $T_4$, $H_3$, and Lander substitutional geometries.[1–3] Thus, all the ordered Al overlayers are characterized by threefold coordination of the Al (in the $\sqrt{7}\times\sqrt{7}$ case, two localized and one delocalized state) which provides for a closed valence shell with only a small amount of charge transfer in each case. In all cases, the Al hybridization provides for an additional unoccupied $p_z$-like state. Various calculations[1,2] show that the $p_z$-like nature of this state is retained for different bonding geometries and Al coverages, although at the highest coverages interactions between neighboring atoms become important. It is this fact which allows us to identify the protrusions observed in positive-bias STM images with the positions of the Al atoms. The strong spatial localization and the insensitivity of the energy of this lowest-energy unoccupied state with coverage show that it plays only a minor role in the

transition from semiconducting to metallic behavior.

This transition is instead determined primarily by the *occupied* electronic states, which show significant changes in both character and energy with increasing Al coverage. At the lowest coverage, these occupied states arise from strong covalent Al—Si bonds. At $\frac{3}{7}$ ML the decreased Al coordination and lateral Al-Al interactions give rise to the cooperative state with energy near $-0.9$ eV. Finally, at 1 ML, as the Al substitutes into the outermost double layer of the Si(111) lattice, the highest-lying occupied electronic states become spatially delocalized and provide significant state density at $E_F$, making the overlayer metallic.

A direct comparison of these findings with previous experimental measurements is difficult, since the majority of these earlier studies were performed by evaporation of Al onto a room-temperature (or below) substrate. Under those conditions the atomic rearrangements necessary to form the ordered overlayers is not always possible. Given the complex electronic structure of the starting Si(111)-$(7\times7)$ surface, achieving a detailed microscopic understanding of the electronic properties of such room-temperature interfaces will be quite difficult.

In summary, we have demonstrated how the local coverage affects the atomic bonding geometry and electronic structure of a prototypical metal-semiconductor system. The equilibrium bonding geometry is determined by a number of factors including minimizing the number of Si dangling bonds, optimizing the tetrahedral geometry for Si, and minimizing repulsive dipolar interactions caused from charge transfer from Al to Si. These changes in atomic geometry are directly related to changes in the local electronic structure, which changes from semiconducting at low coverages to metallic at a coverage of $\simeq 1$ ML.

## ACKNOWLEDGMENTS

The author gratefully acknowledges useful discussions with J. E. Demuth and U. Kohler. This work was supported in part by the U.S. Office of Naval Research.

[1]J. E. Northrup, Phys. Rev. Lett. **53**, 683 (1984).
[2]H. Nagayoshi, in *Dynamical Processes and Ordering on Solid Surfaces* (Springer-Verlag, Berlin, 1985).
[3]J. R. Chelikowsky, Phys. Rev. B **16**, 3618 (1977).
[4]H. I. Zhang and M. Schlüter, Phys. Rev. B **18**, 1923 (1978).
[5]J. J. Lander and J. Morrison, Surf. Sci. **2**, 553 (1964).
[6]J. E. Demuth, R. J. Hamers, R. M. Tromp, and M. E. Welland, J. Vac. Sci. Technol. A **4**, 1320 (1986).
[7]R. J. Hamers, R. M. Tromp, and J. E. Demuth, Phys. Rev. Lett. **56**, 1972 (1986).
[8]N. D. Lang, Phys. Rev. Lett. **58**, 45 (1987).
[9]R. M. Feenstra, J. A. Stroscio, and A. P. Fein, Surf. Sci. **181**, 295 (1987).
[10]R. J. Hamers, Ph. Avouris, and F. Bozso, Phys. Rev. Lett. **59**, 2071 (1987).
[11]T. Kinoshita, S. Kono, and T. Sagawa, Phys. Rev. B **32**, 2714 (1985).
[12]G. V. Hansson, R. Z. Bachrach, R. S. Bauer, and P. Chiaradia, Phys. Rev. Lett. **46**, 1033 (1981).
[13]R. I. G. Uhrberg, G. V. Hansson, J. M. Nicholls, P. E. S. Persson, and S. A. Flödstrom, Phys. Rev. B **31**, 3805 (1985).
[14]B. N. Dev, S. M. Mohapatra, K. C. Mishra, W. M. Gibson, and T. P. Das, Phys. Rev. B **36**, 2666 (1987).
[15]M. Kelly, G. Margaritondo, J. Anderson, D. J. Frankel, and G. J. Lapeyre, J. Vac. Sci. Technol. A **4**, 1396 (1986).
[16]R. J. Hamers and J. E. Demuth, J. Vac. Sci. Technol. A **6**, 512 (1988).
[17]J. M. Nicholls, B. Reihl, and J. E. Northrup, Phys. Rev. B **35**, 4137 (1987).
[18]R. J. Hamers and J. E. Demuth, Phys. Rev. Lett. **60**, 2527 (1988).
[19]T. Kinoshita, S. Kono, and T. Sagawa, Solid State Commun. **56**, 681 (1985).
[20]K. C. Pandey, Phys. Rev. Lett. **47**, 1913 (1981).
[21]J. E. Northrup, Phys. Rev. Lett. **57**, 154 (1986).
[22]J. S. Nelson and I. P. Batra, in *Proceedings of the NATO Advanced Research Workshop on Metallization and Metal-Semiconductor Interfaces* (Plenum, New York, in press).
[23]N. D. Lang, Phys. Rev. B **34**, 5947 (1986).
[24]R. J. Hamers, J. Vac. Sci. Technol. B **6**, 1462 (1988).
[25]J. Stroscio, R. Feenstra, and A. P. Fein, Phys. Rev. Lett. **57**, 2579 (1986).
[26]R. S. Becker, T. Klitsner, and J. S. Vickers, Phys. Rev. B **38**, 3537 (1988).
[27]M. D. Pashley, K. W. Haberern, and W. Friday, J. Vac. Sci. Technol. **6**, 488 (1988).
[28]D. Bolmont, P. Chen, and C. A. Sabenne, J. Phys. (Paris) Colloq. **45**, C5 (1984).
[29]W. Telieps and E. Bauer, Surf. Sci. **162**, 163 (1985).
[30]M. Kelly, G. Margaritondo, L. Papagno, and G. J. Lapeyre, Phys. Rev. B **34**, 6011 (1986).
[31]F. K. LeGoues, W. Krakow, and P. S. Ho, Philos. Mag. A **53**, 833 (1986).
[32]A. Zur and T. C. McGill, J. Appl. Phys. **55**, 378 (1984).
[33]J. E. Demuth, U. K. Köhler, R. J. Hamers, and P. Kaplan, Phys. Rev. Lett. **62**, 641 (1989).
[34]M. Kelly, E. Colavita, G. Margaritondo, J. Anderson, L. Papagno, D. J. Frankel, and G. J. Lapeyre, Phys. Rev. B **32**, 2693 (1985).

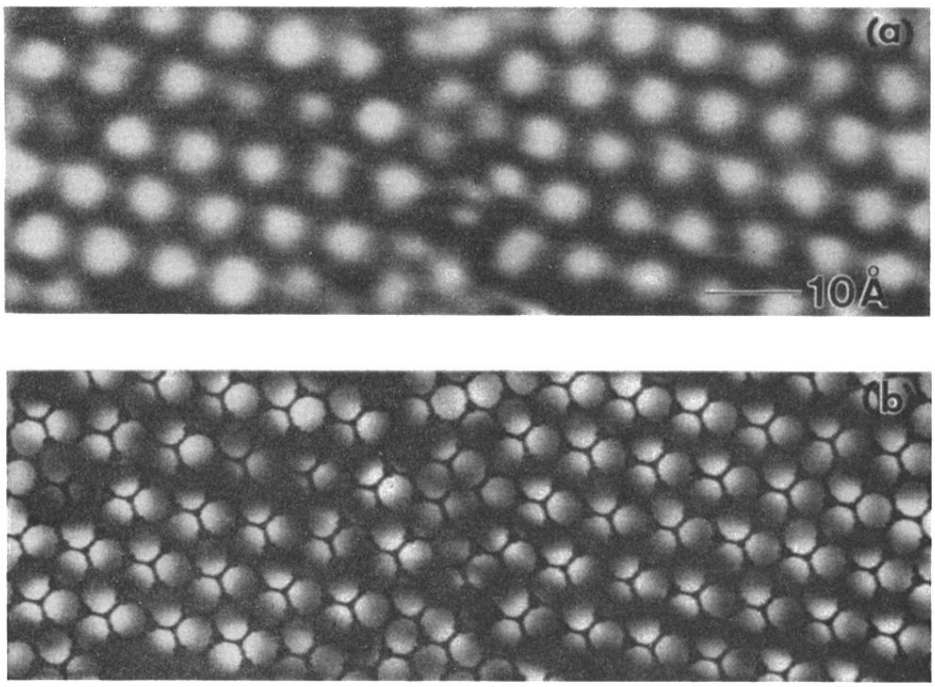


FIG. 1. (a) STM topographic images of Si(111)-($\sqrt{3}\times\sqrt{3}$)Al including a boundary between two domains. (b) Same image as in (a), but now with a hexagonal lattice superimposed.

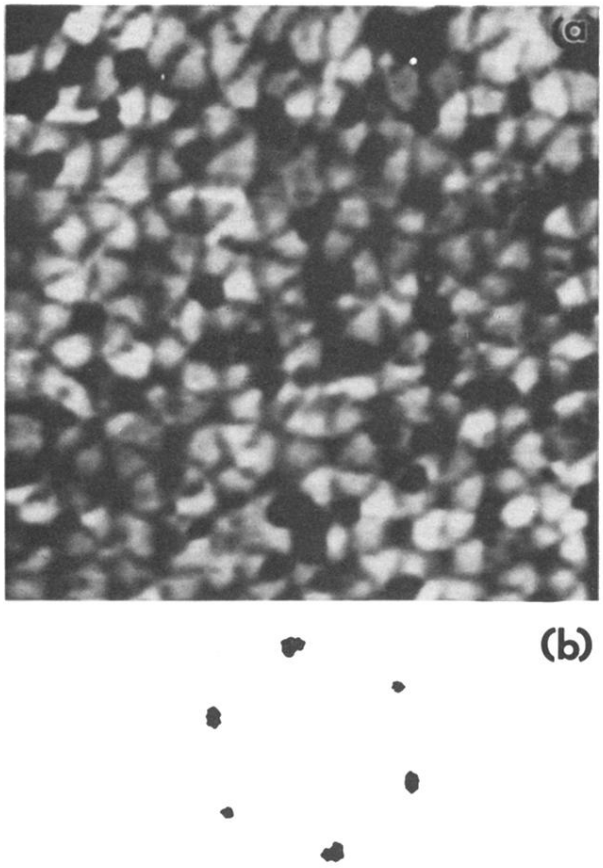


FIG. 10. Tunneling results for Si(111)-(7×7)Al structure at 1 ML coverage: (a) large-area scan, +1.5 eV sample bias; (b) two-dimensional fast Fourier transform of image shown in (a).

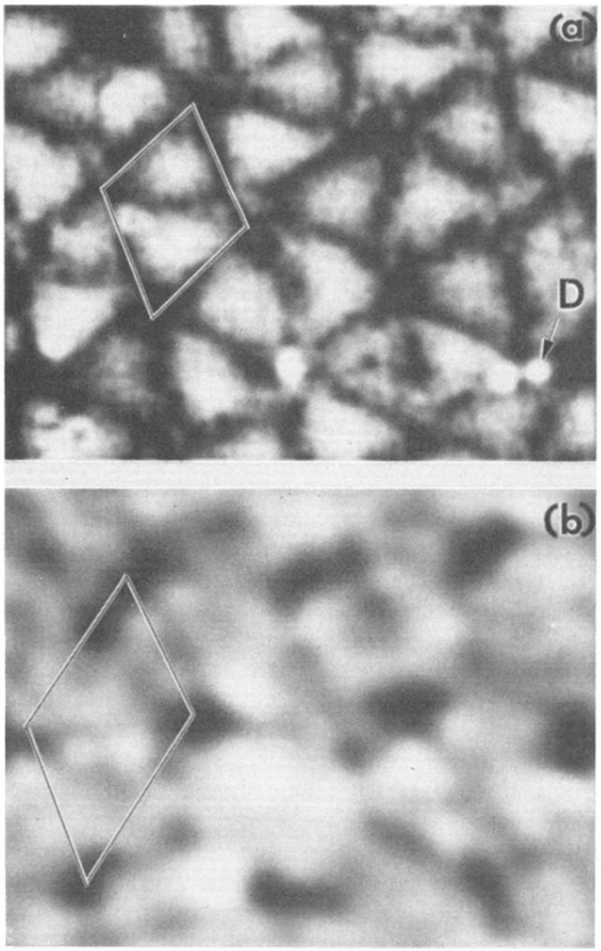


FIG. 11. High-resolution STM topographs of Si(111)-(7×7)Al: (a) high-resolution scan, +1.5 eV sample bias; (b) high-resolution scan, −1.2 eV sample bias.

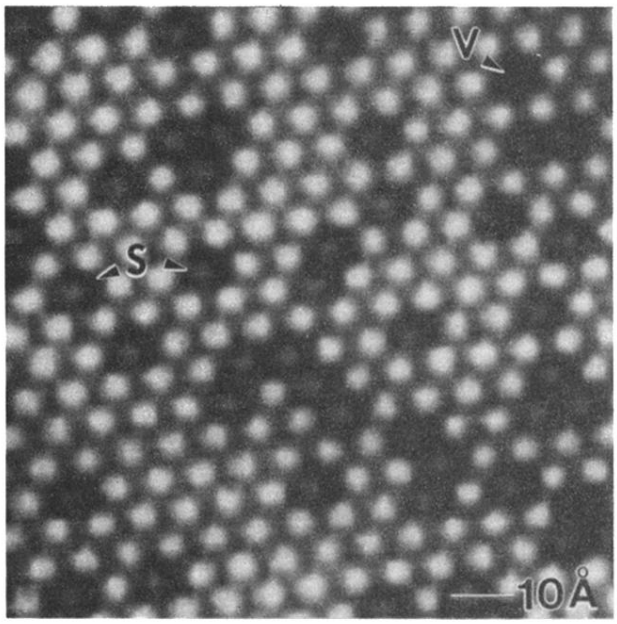


FIG. 2. STM topographic image of Si(111)-($\sqrt{3}\times\sqrt{3}$)Al including Si substitutional defects (+1.2 eV sample bias).

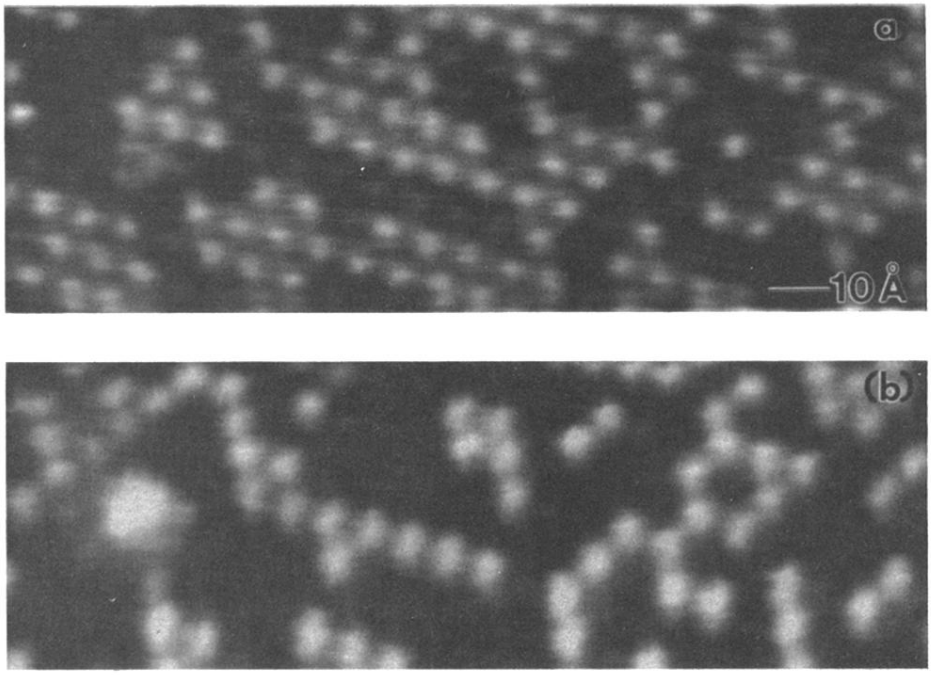


FIG. 3. STM topographic image of a single region with $\frac{1}{6}$ ML Al coverage. The local nature of the $\sqrt{3}\times\sqrt{3}$ bonding permits selective imaging of (a) Al adatoms at positive sample bias and (b) Si adatoms at negative sample bias.

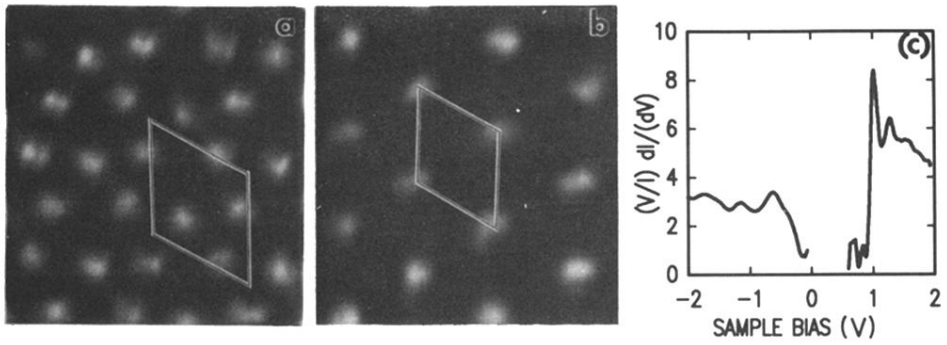


FIG. 5. Constant-current topographs of Si(111)-($\sqrt{7}\times\sqrt{7}$)$R$ 19.1° structure at positive [(a), +1.6 V)] and negative [(b), −1.6 V] bias, and results of tunneling-spectroscopy measurements [(c)].

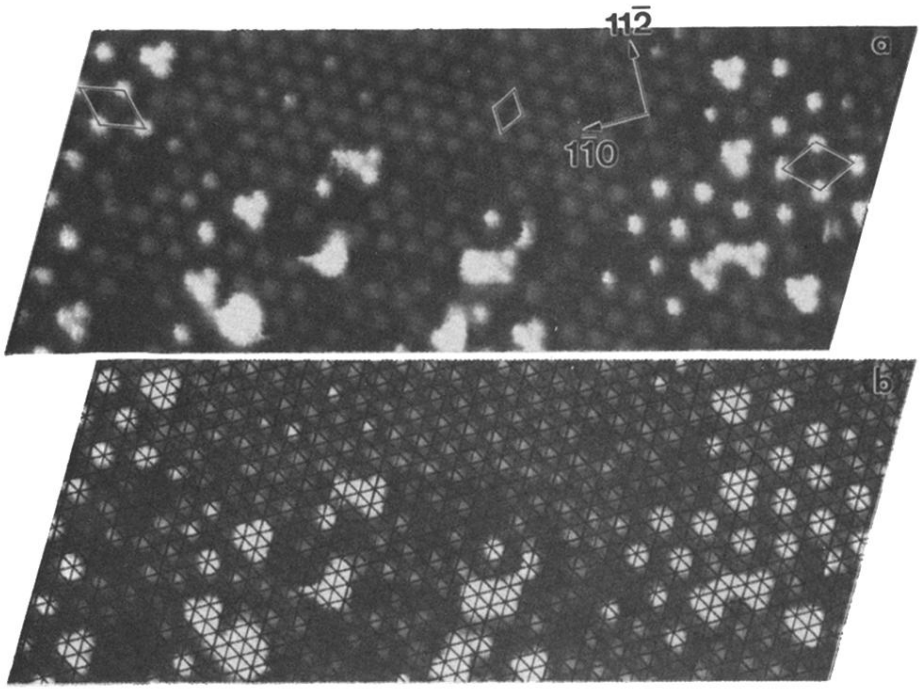


FIG. 6. domain boundary between $\sqrt{3}\times\sqrt{3}$ (center) and $\sqrt{7}\times\sqrt{7}$ (left and right) structures, obtained at sample bias of $-1.6$ eV.

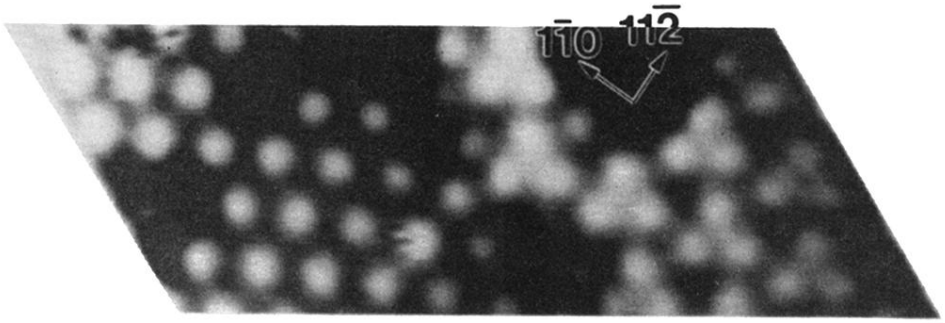


FIG. 7. Domain boundary between $\sqrt{3}\times\sqrt{3}$ (left) and $\sqrt{7}\times\sqrt{7}$ (right) structures, obtained at sample bias of $+1.6$ eV. Crystallographic orientations are given.

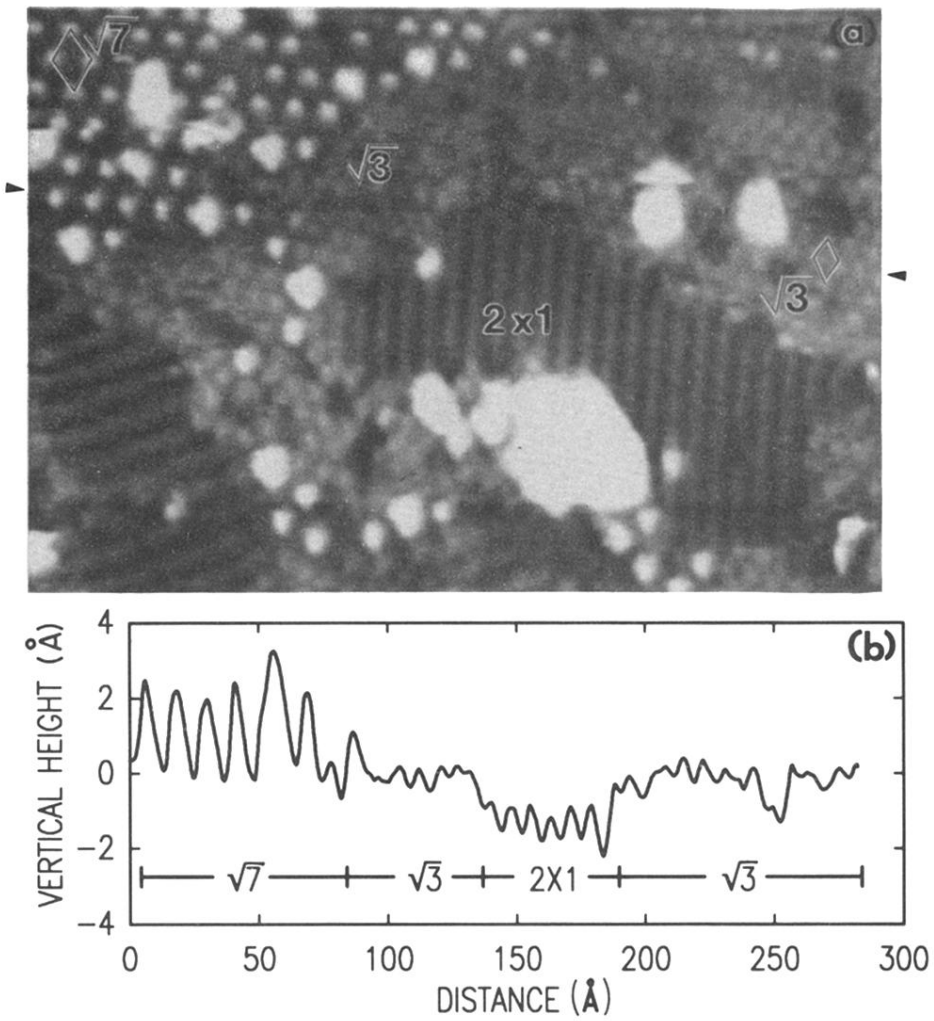


FIG. 9. (a) STM images showing two domains of (2×1) structure coexisting with ($\sqrt{3}\times\sqrt{3}$)Al [surrounding (2×1) regions] and $\sqrt{7}\times\sqrt{3}$ (top left) structures. Arrows denote starting and ending points for (b), the corrugation profile over the various superstructures observed in (a).